Lunar pilot plant payload design toward in situ demonstration of oxygen extraction by carbothermal reduction.

Alice Dottori⋆†, *Ivan Troisi*⋆, *Michele Roberta Lavagna*⋆, *Simone Pirrotta*⋆⋆ *and Francesco Latini*⋆⋆
⋆*Politecnico di Milano*
Via La Masa, 34 Milano, Italy
alice.dottori@polimi.it · ivan.troisi@polimi.it · michelle.lavagna@polimi.it
⋆⋆*Agenzia Spaziale Italiana*
Via del Politecnico, Italy
simone.pirrotta@asi.it · francesco.latini@asi.it
†Corresponding author

11/06/2023

Abstract

The laboratory success of carbothermal reduction of solid regolith for water production[26] has led to the proposal of a pilot plant for validation in the lunar environment. The Italian Space Agency (ASI) plans to allocate a slot on a commercial lunar lander to showcase an in-situ resource utilization (ISRU) process. Multiple architectures have been proposed to demonstrate the process while fulfilling the lander's requirements. These architectures are based on an analysis of plant functionalities, with a focus on key components. Thermal analysis highlights power as a critical resource with potential solutions to maintain the required reaction temperature. The challenges of miniaturization for fluidics are also addressed.

1. Introduction

In the coming years, the surface of the Moon is foreseen to be crowded by crewed and robotic missions. The capability to exploit local resources, especially the regolith, is a key point in carrying on a sustainable long-term lunar exploration. In-Situ Resource Utilization (ISRU) processes that extract or produce oxygen from the regolith are being extensively studied. Among the numerous methodologies,[29] the most promising ones include carbothermal reduction of molten[11] or solid[26,31] regolith, and FFC Molten Salts Electrolysis.[21] Some of these processes have advanced from breadboarding experiments to terrestrial demonstrator plants. The next step involves demonstrating these processes in a representative environment, such as the lunar surface, similar to the MOXIE experiment conducted on Mars.[15] The Italian Space Agency (ASI), which has among its key interests the development of such demonstration assets, plans to allocate a slot on a commercial lunar lander (around 15 kg) to demonstrate an ISRU process.

So, this paper discusses the roadmap towards feasibility for the solid carbothermal reduction plant, as adopted by the ASTRA team at Politecnico di Milano (PoliMi). The discussion is based on the experience gained from a test campaign conducted from 2018 to 2021 on a demonstrator plant,[26] which was built as part of an ESA-financed study. The proven carbothermal reduction is a two-stage solid-gas reaction that gets water from a methane/hydrogen mixture fluxed on a lunar simulant, which reduces the feedstock at temperatures lower than the simulant melting point, such as $1100\,°C$ for a highland soil. This procedure is still effective to trigger the oxygen removal as carbon oxides, preventing the handling of a high-temperature molten phase. The methanation stage converts the gases exiting from the previous reactor, nominally CO, CO_2, H_2 and CH_4 into water vapour and again CH_4 and H_2. The water vapour is condensed, while the gases can be reused in the cycle with a dedicated gas separation unit currently under study but not included in this design. No or minor feedstock beneficiation is requested, greatly simplifying the plant operations automation; furthermore, the solid phase helps in an easier discharge procedure. The laboratory plant, to be miniaturized towards flight, includes two reactors, two feeding lines and tanks, a condenser, actuators and sensors to control the flow and quantify the gaseous species. The extent of the process demonstration depends on the mass and volume budget allocated for the purpose, as well as other constraints, which will be described in detail throughout the paper. For example, the need for a dedicated sampling mechanism or robotic arm may reduce the available mass for a full demonstration of

LUNAR ISRU PILOT PLANT DESIGN

Table 1: CLPS providers table, with the indication of the constraints in terms of mass, power and surface/volume available

Company Name	Lander Name	Available Mass	Available Power	Available surface or volume and location
Astrobotic[2]	Peregrine	70-90 kg	1-2.5 W/kg	0.2-0.5 m^2, very flexible locations
	Griffin	625 kg	1-2.5 W/kg	For rover/large payloads
Draper[8]	Artemis-7	16-30 kg	102-241 W	Top of the lander, deliverable on the surface
Firefly[10]	Blue Ghost	10-50 kg	38-300 W	0.38x0.13x0.23 to 0.69x0.45x0.65 m
Intuitive machines[16]	Nova-C	7.7-100 kg	2-300 W	0.054-0.468 m^2
Masten[20] (acquired by Astrobotic in 2022)	XL-1	2bays*50 kg	50 W/bay	0.787x0.610x0.610 m, lander bottom
Lockheed Martin Space[19]	McCandless Lunar Delivery Service	350 kg	400 W	4 m^2 at 0.9 m height
Moon Express[23]	MX-1 to MX-9	30-500 kg	200 W	N/A
Blue Origin[4]	Blue Moon	4000 kg	N/A	N/A
Ceres Robotics[7]	B5 lander	N/A	N/A	N/A
Sierra Nevada Corporation	N/A	N/A	N/A	N/A

the process. To carry out this demonstration, the NASA Commercial Lunar Payload Services (CLPS) program offers the most promising opportunity for enhancing such technologies. The challenge lies in reducing the size of a complex chemical plant while maintaining adequate performance and complying with CLPS constraints.

This article provides an overview of the main CLPS opportunities for reaching the lunar surface and then focuses on the carbothermal process and possible strategies for its demonstration. It presents a functional analysis of the plant, including its constituent blocks, and compares the potential architectures of the demo plant with respect to the limitations imposed by the lander. Finally, a more detailed analysis of crucial plant components is presented.

CLPS investigation. In Table 1 are reported the principal companies and CLPS landers with the public-available characteristics in terms of available mass, power and surface. While most providers can meet the ASI-proposed allocation of 15 kg in terms of mass and volume, there are limitations in terms of power. The process requires more than 60 W of power, so some of the providers like Astrobotic and Masten have to be discarded unless stipulating different agreements. Regarding the landing sites, there is strong flexibility in the selection, going from the poles to the near side:[25]

- **Near-side**: Oceanus Procellarum (Intuitive Machine, 2023); Lacus Mortis (Astrobotic, 2023); Mare Crisium (Firefly, 2024); Reiner Gamma (PRISMA 1 on Intuitive Machine, 2024); Schrödinger crater (PRISMA 1 on Draper, 2025); Gruithuisen Domes (PRISM 2, 2025).

- **South Pole**: PRIME-1 on Intuitive Machine, 2023; Masten (Astrobotic), 2023; VIPER rover, Astrobotic, 2024.

It is also interesting to grasp the criteria used by NASA to gather different payloads: indeed this aspect can be useful to understand if a sampling mechanism is already on board, and if it is a common request so that they are already provided by the lander. Looking at the PRISM calls,[24] PRISM 1 and 2 do not need any sampling mechanisms, as they will focus on magnetic, seismic, spectroscopy and biology applications. In PRISM 3, instead, it is clearly specified that a sample acquisition mechanism increases the cost and complexity, with the main concerns being the contamination control and the interfaces, so this service is not offered as a vendor-provided service. Thus, it is reasonable to envisage also the presence of a sampling mechanism in the payload. This aspect makes even more crucial to design the lunar demonstrator and the operations to perform in an optimal way, minimizing the mass but maximising the results. In general, the payload complexity is also part of the evaluation process, so the simpler the operations to achieve the science objectives, the easier the acceptance process.

2. Carbothermal process design

The knowledge gained from the 2018-2021 test campaign[26] is leveraged to design the strategy for carbothermal reduction in the pilot plant. The critical chemical parameters are established to maximize the oxygen yield of the process. The optimum temperature (T_{CRB}) for the carbothermal reduction of the NU-LHT-2M simulant[31] is 1100 °C; depending on the landing site, adjustments may be made to maximize the yield while preventing the batch from melting, and a lower reaction temperature may be targeted for the maria regolith. The mixing ratio of H_2/CH_4 and the inlet mixture

Table 2: Carbothermal process possible strategies. The number of process repetitions is labelled on the strategy name *single* or *multi*. For the exhaust regolith management: *S* stacked, new regolith loaded on top of the old one, *D* exhaust regolith is discharged. For the process alternation the following scheme is followed: *a*: M1(3 h)+W1(5 h), *b*: M1(3 h)+W1(5 h) +M2(3 h)+W2(8 h) +M3(3 h)+W3(9 h), *c*: M1(3 h) +W1(5 h) +M2(3 h) +W2(8 h) +M3(3 h) +W3(9 h) +M4(3 h) +W4(10 h) +M5(3 h) +W5(10 h) +M6(3 h) +W6(12 h) +M7(3 h) +W7(10 h).

	Repetitions	Exhaust	t_P [h]	Alternations	Heating gas	# tanks
M-3h-single	1	-	3	-	H_2+CH_4	1
M-7h-single	1	-	7	-	H_2+CH_4	1
M-3h-multi$_S$	2+	S	3	-	H_2+CH_4	1
M-7h-multi$_S$	2+	S	7	-	H_2+CH_4	1
MW-8h$_a$-single	1	-	8	a	H_2	2
MW-31h$_b$-single	1	-	31	b	H_2	2
MW-85h$_c$-single	1	-	85	c	H_2	2
MW-8h$_a$-multi$_S$	2+	S	8	a	H_2	2
MW-31h$_b$-multi$_S$	2+	S	31	b	H_2	2
MW-85h$_c$-multi$_S$	2+	S	85	c	H_2	2
MW-8h$_a$-multi$_D$	2+	D	8	a	H_2	2
MW-31h$_b$-multi$_D$	2+	D	31	b	H_2	2
MW-85h$_c$-multi$_D$	2+	D	85	c	H_2	2

flow rate are set at 85%/15% and 0.5 L/min respectively, and are considered fixed. The mass of regolith loaded into the reactor (m_{REG}) impacts the process yields and directly influences the size of the plant, therefore, it remains a core parameter for sizing.

Process strategies. Defining the process strategy involves determining the alternating scheme between H_2/CH_4 and H_2-only phases, along with the process duration. Additionally, the number of process repetitions and, if needed, the management of the exhaust regolith batch are considered. The phase alternating scheme drives the choice of the gas to be flown during the heating phase of the plant and the number of tanks required for the gas storage. When possible, H_2 is flown during the heating phase, to trigger also lower-temperature reactions such as the ilmenite reduction;[28] in the case of a short strategy, instead, the pre-mixed H_2 + CH_4 is exploited, so that only a tank is needed. However, the carbon deposition during the heating can produce effects that need to be assessed during the planned breadboarding activities of the scaled process.

Table 2 summarizes the process strategies investigated. The names of the strategies reflect their characteristics, reported in the related columns. Three alternation schemes, corresponding to different process durations, are explored: the first (*a*) includes one mixture and one H_2-only phases, the second (*b*) is an intermediate strategy which lasts for three complete alternations, while the third one (*c*) plans seven phases alternation in order to maximise the oxygen extraction. Those values are based on the expected process yield and coke deposition rate modelled in the 2018-2021 experimental campaign on the terrestrial plant. The duration and alternating phases guide the mass of gases required for the process, which impacts the plant mass budget and configuration. The baseline duration of the different phases is set arbitrarily to maximise the oxygen yield while avoiding the full consumption of the deposited coke in the regolith batch, and so targeting a constantly increasing yield for all the phases. When multiple processes are planned, the strategy for handling the exhaust regolith differs. It can either involve stacking fresh regolith on top of the processed one without discharging (*S*), or removing the exhaust regolith from the carbothermal reactor (*D*). The latter option requires the introduction of an unloading valve, increasing complexity. Still, it allows for minimizing the reaction dimensions to accommodate only the targeted mass of regolith needed for the process.

Process sizing. The quantity of gas required to complete the process is computed once the alternating scheme is defined. The mass of hydrogen and methane is determined by integrating their molar fluxes using equation 1, where x_i [-] represents the gas molar fraction, fl [mol/s] is the total molar flux, and MW_i [g/mol] is the molar mass. The volume of the gases is then considered, assuming pressurization within the range of 200–300 bar.

$$m_i = MW_i \int_0^{t_p} x_i \, fl \, dt \quad i = H_2, CH_4 \tag{1}$$

To provide an initial estimation of tank dimensions and masses, cylindrical ($r/h = 1/3$) Ti_6AlV tanks are designed based on strength. The wall thickness t_{TANK} is computed using equation 2, which takes into account the pressure inside the tank P_{tank} [Pa], the radius r_{tank} [m], and the ultimate tensile stress of the material σ_{TU} [N/m^2]. This process allows

for a direct linkage between the process duration, yield, and the mass budget of the plant, as illustrated in Figure 1.

$$t_{\text{tank}} = \frac{P_{\text{tank}} r_{\text{tank}}}{\sigma_{\text{TU}}} \qquad (2)$$
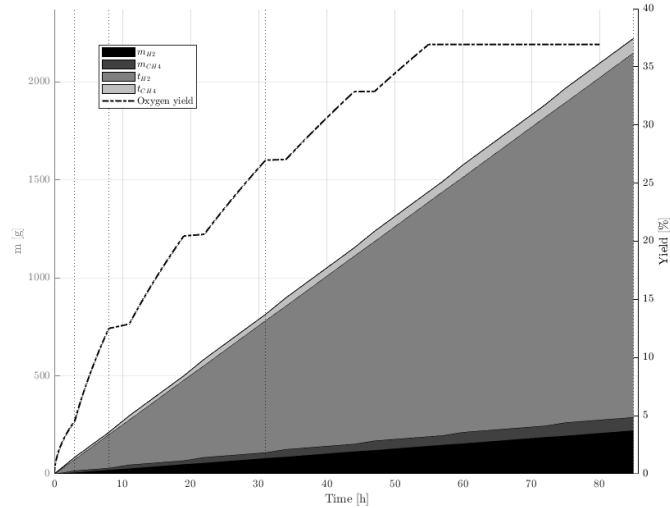
Figure 1: Carbothermal process sizing: gases and tanks mass evolution concerning the process duration. Alternation scheme c from Table 2 is considered and cylindrical Ti$_6$AlV tanks with a radius-to-height ratio of 1/3 and P_{H2}=300 bar, P_{CH4}=200 bar considered for the tank sizing. Yield trend shown with the dashed line, for a 30 g batch, 0.5 L/min flux.

Process yield. The knowledge acquired from the 2018-2021 test campaign allows to retrieve the process yield from the input gases by modelling the kinetics of the solid-gas carbothermal reduction. The modelling is performed using the data collected from the tests, in particular the gases concentration acquired with a gas chromatographer: these values are useful to tune the kinetic parameters to be used in the kinetic model. A detailed description of the models is under publication. From that the oxygen yield, defined as in Eq. 3, is computed as the ratio between the O$_2$ extracted downstream of the carbothermal reduction and the oxygen originally available in the regolith batch, assumed to be 45% of the total mass of regolith.[14] The variation of the yield with respect to the process strategy is shown in the dashed line of Figure 1, where the c strategy is adopted and 30 g of mass are considered for the regolith batch with a flux of gases of 0.5 L/min.

$$yield = \frac{m_{O2,EXTRACTED}}{0.45 m_{REG}} \qquad (3)$$

3. Pilot plant preliminary design

The architecture of the plant is defined once the boundaries of the process parameters investigations are set. The components are identified from the functional analysis, and are then exploited to propose different architectures.

3.1 Functional analysis

The primary functionality of the plant is to demonstrate the carbothermal reduction of solid regolith in the lunar environment. Additionally, the pilot plant aims to showcase the necessary technology for conducting the process and measuring its outputs. Figure 2 illustrates the six main functional blocks:

- *Carbothermal reduction.* This block shall support and facilitate the carbothermal reduction in the lunar environment by providing the required power, insulation, and sealing capabilities. It shall host the regolith batch, allowing its loading and, if required, unloading. The process gases shall be flown inside the reactor and the gaseous products shall exit towards the other plant components.
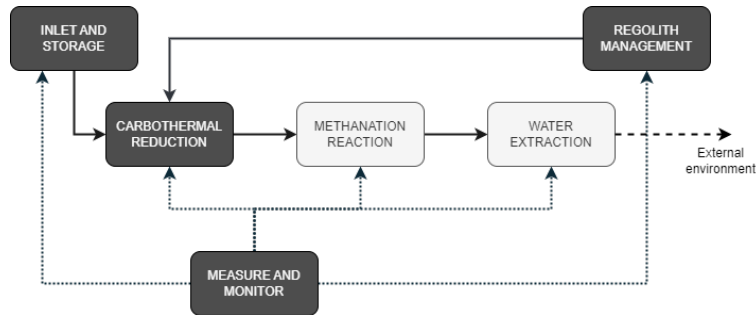
Figure 2: Lunar pilot plant functional scheme

- *Methanation reaction:* Since the product of the carbothermal reduction is CO, this block is needed to convert it into water, which is the final output of the plant. The block sustains and facilitates the reactions, allowing for the inflow and outflow of gases and accommodating a catalyst to promote the reactions if required by the selected conversion technology. The reaction conditions shall be granted and monitored.

- *Water extraction.* This block aims to separate the water from the gaseous mixture, enabling its storage or discharge into the environment. The required conditions for the water separation shall be granted, while the non-condensed gases instead shall be able to re-enter the fluidics block to manage their discharge.

- *Measure and monitor.* This block is responsible for monitoring the outputs of the carbothermal reactor, particularly the quantity of CO produced. It also includes the monitoring of the products from the methanation and condensation stages, if present, as well as the overall status of the plant. Moreover, it evaluates the mass of regolith loaded inside the reactor and monitors plant pressure and temperature conditions.

- *Inlet, fluidics and storage.* This block ensures the proper flow of reactants into the plant in the correct ratio and their storage during all the mission phases. It is monitored by the *Measure and monitor* block. Furthermore, it minimizes dangerous situations by active and passive components, like flame arrestors and no-return valves.

- *Regolith management.* Depending on the chosen lander, it may be necessary to directly collect the required amount of regolith from the lunar soil. In any case, the regolith needs to be transported to the reactor and loaded inside it while measuring the batch mass. Additionally, depending on the process strategy, the capability to discharge the regolith from the reactor towards the external environment or a dedicated container in the plant might also be required.

3.2 Principal Plant Components

The key components required to achieve the different functionalities are identified for each block.

Carbothermal Reduction. A reactor is necessary to host the carbothermal reduction; its dimensions are determined by the mass of the regolith batch to be processed, as well as the constraints imposed by the lander. The reactor shall have fluidic interfaces, and it shall be equipped with at least one aperture for the regolith loading. Depending on the exhaust regolith management strategy, a second aperture might be necessary for batch discharge. Sealing against gases and regolith particles is achieved through a careful design of the reaction chamber, including flanges for gas sealing and particle filters. An accompanying oven shall provide the required heat for sustaining the reduction temperature, and it interfaces with the lander power management system. Insulation of the assembly can be considered to minimize thermal losses and power requirements. A potential configuration, which will be further explored in subsequent trade-off analyses, involves a cylindrical reactor heated by heating coils and wrapped in one or more layers of insulation. The radius-to-height ratio can be adjusted to minimize both the mass and thermal losses. Similarly, the thickness of the insulating layers should be optimized.

Methanation Reaction. Different concepts have been demonstrated in space to convert carbon oxides in water, such as solid oxide electrolyzer cells[13] and microchannel reactors[17] and the catalytic Sabatier reactor demonstrated on the International Space Station.[27] Those architectures can be traded off to include this block in the pilot plant, as its presence would allow the full process demonstration. The baseline configuration of the methanation reactor is similar to

the carbothermal reactor, consisting of a hollow cylinder wrapped in heating coils, potentially with additional insulation layers if required. The reactor hosts a catalyst to promote the reaction and interfaces with the plant fluidics for the inflow and outflow of process gases. The length of the reactor ensures complete conversion of CO into water and methane given the pressure and temperature conditions. The shape of the catalyst pellets will be chosen to maximize efficiency and achieve full conversion of CO.

Water extraction.   Various technologies can be exploited to extract water vapour from the mixture, including condensers, gravity separators, corrugated plates, cyclone separators, swirl tubes, and filters.[12] As a baseline, condensation is the considered technology given the lunar operative environment. The condenser is the core component of the block: it can either be submerged in a freezer or exploit the lunar environment and the lander thermal interfaces to achieve the required operating temperature. The presence of this block depends on the inclusion of the methanation block: without it, the condensation block would serve no purpose. However, if water vapour is produced from ilmenite reduction by hydrogen or by heating the possible trapped ice, the presence of the condensation block can be considered.

Measurement and Monitoring.   Accurate measurement and monitoring are crucial for ensuring the efficiency and effectiveness of the plant. Various sensors are employed to assess the key parameters and provide real-time data for analysis. Downstream of the carbothermal reactor, a sensor is placed to measure the concentration of CO, which serves as an indicator of the reduction status. Additional sensors shall be strategically positioned within the plant to measure methane and carbon monoxide and monitor the mixture composition. Pressure and temperature sensors are also installed at critical locations to monitor the status of the components and ensure optimal operation. The selection of sensors is based on Commercial Off-The-Shelf (COTS) components but customization of sensors designed for terrestrial applications is also considered. Accurately determining the mass of the regolith batch is critical as it directly impacts the process yield. Several technologies can be employed for this purpose, including mass balances and load cells that can weigh either the regolith in the regolith management block or the loaded reactor. Another approach involves estimating the volume of the loaded regolith and calculating the mass based on density. To accomplish this, a graduated reactor can be utilized if equipped with a camera, or level sensors can be employed. Incorporating the condensation functionality requires the inclusion of a component to measure the mass of the obtained water. Furthermore, instruments for studying water properties can be included for in-depth analysis. An additional camera can be installed to capture images of the produced water and the regolith before and after the process.

Inlets, Lines, and Storage.   Pipes are essential for interconnecting the different elements of the plant. Their length should be minimized to reduce mass and pressure losses, while ensuring they can withstand the operating pressure and process gases. Along the pipes, various components such as anti-return valves, flame arrestors, and check valves are installed to monitor and control the flow. Flowmeters and pressure reducers are required at the interface between the tanks and the lines to achieve the desired operating pressure and nominal mixture composition. For storing the process gas, one or two high-pressure tanks are necessary. The previous section provided an initial estimation of the mass, but the evaluation of Commercial Off-The-Shelf (COTS) components should be considered.

Regolith Management.   Loading the regolith into the reactor may require a horizontal and vertical transportation system, depending on the configuration of the lander. Belts, augers, and traditional vibratory conveyors can be utilized, taking into account the poor flowability of lunar regolith.[6] To minimize regolith dispersion during loading, a funnel-like component could be employed, placed on the loading valve of the carbothermal reactor. A sieve could be employed to monitor the size distribution of the regolith grains. If the carbothermal reactor needs to be emptied, appropriate mechanisms should be implemented to facilitate the movement and discharge of the exhaust regolith, considering its poor flowability exacerbated by the absence of atmosphere and the electrostatic charges that encourage particles to adhere to surfaces.[6] Two scenarios are possible for the acquisition of the regolith batch: either the lander is equipped with a sampling mechanism and it is necessary to transport the regolith and load in the reactor or there is no regolith acquisition/management subsystem on the lander and it is necessary to design the full subsystem. If the regolith batch is not provided by the lander, a tool for acquiring regolith samples is necessary. Depending on the required mass of regolith, the height with respect to the soil, and the lander configuration and budget, various solutions can be adopted.[3, 18, 35] Drills, scooping, and shovels are high Technology Readiness Level (TRL) solutions commonly used for surface regolith acquisition, although the latter two may require the use of a robotic arm.

3.3 Proposed architectures

Selecting the baseline demo plant architecture involves defining the process strategy and identifying all the plant components and their preliminary configuration. The process strategies proposed in Table 2 pose some requests on the

mass, power and volume budgets for the different architectures and requirements for their definition. The choice of the architecture considers the following factors: the mass of regolith to be processed, m_{REG}; the process strategy; the presence of the methanation block; the presence of the water extraction unit; and the presence of a regolith sampling mechanism. Other plant components, such as the regolith transportation mechanism, measurement instruments such as the CO detector, and the plant sensors, are required in all the solutions. The trade-off criteria for architecture selection include plant mass, power budget, scientific return, and plant complexity.

The preliminary mass budget is computed for the different process strategies presented in Table 2, considering both a plant with mandatory components only (without methanation, water extraction, and regolith sampling elements) and the full plant. Figure 1 shows the dependence of the mass of gases and tanks with respect to the alternation strategy. The mass of the carbothermal reactor is estimated by a parametrization of its geometry with respect to the mass of the regolith batch. A cylindrical reactor made of alumina (ρ_C =1950 kg/m^3) and two layers of silica and carbon aerogel insulators (ρ_{CA} =10 kg/m^3, ρ_{SA} =150 kg/m^3) is considered, with each insulator layer having an arbitrary thickness of 10 cm. The inner radius of the chamber is arbitrarily set to 2.5 cm, and the height of the cylindrical chamber is set to be 2.5 times the height of the regolith column. Inlet and outlet regions with 55° inclinations are considered. The methanation reactor is sized accordingly, assuming a length of 8 cm to ensure the full CO conversion, and an insulant layer of thickness 2 cm, with an estimated total mass of 0.5 kg. The mass of the condenser is arbitrarily assumed to be 600 g, based on downsizing the solution adopted in the laboratory plant.[26] Similarly, a mass of 1 kg is assumed for the regolith management subsystem, considering the preliminary information available. The thermal control subsystem (TCS), fluidics, onboard data handling, and power control system are estimated based on the payload mass. The power budget is driven by the carbothermal stage and its power demand to heat the regolith batch to the reduction temperature. The methanation reactor and water extraction unit power request are foreseen to be minimized through the exploitation of passive heating and cooling, and it does not enter the preliminary trade-off considerations. Similarly, the power request of the sensors and other subsystems is expected to be almost independent of the architecture choice. The scientific return is mainly dependent on the process yield, which is higher the longer the process duration. Moreover, the scientific value increases when the full process, including liquid water storage, is demonstrated as well as the processing of multiple batches. The plant's complexity depends on the number of elements required by the architecture, the mechanisms involved, and the planned number of operations for the selected process strategy. For example, the unloading of regolith from the carbothermal reactor leads to higher complexity compared to the batch stacking strategy, where the regolith is not discharged but the new batches are loaded on top of the exhaust ones.

Architectures comparison   Figure 3 illustrates the mass budgets for different possible architectures derived from the parameters mentioned above. The carbothermal (CRB) block is the most massive in all cases, with an increase of 1 kg between the 30 g and 90 g configurations. This increase should be evaluated considering the expected process yield. The fluidic subsystem (FLD) mass is mainly influenced by the process duration due to the quantity of gas required and the large dimensions of the tanks: to them, an estimated mass for the lines and other components are added, leading to making it one of the subsystems with the largest contribution. However, only configurations involving large quantities of regolith, long process durations, or a high number of process repetitions exceed the 15 kg threshold imposed by ASI, and no mass-critical architectures are identified.

The main power demand comes from the carbothermal reactor, which needs to heat the regolith from lunar surface temperature to above 1000 °C. The energy necessary to heat the regolith batch can be estimated as $Q = mc_P\Delta T$, which amounts to 215 kJ for the 30 g batch. A simplified model is used to estimate the thermal losses to the external environment: the resulting power demand is in between 50–120 W, increasing with the mass to be heated. Since power is a crucial resource for the plant, more refined thermal simulations of the carbothermal reactor are performed, as shown in Section 4. The process yield depends upon both the chosen process strategy and its duration. From a scientific standpoint, extending the process duration is preferred due to its potential impact on overall yield, as well as demonstrating the process's repeatability. The complexity primarily arises from managing the exhaust regolith batch in architectures involving multiple process repetitions. In all cases, the loading of regolith into the reactor necessitates a series of well-defined operations including positioning of the regolith transportation/loading mechanism, unsealing the reactor, opening the loading valve, loading the regolith, closing the loading valve, and sealing the reactor. If unloading of the exhaust batch is required, additional operations are necessary: consequently, the inclusion of these additional steps effectively doubles the number of required operations and mechanisms, which does not happen in the case of a stacked strategy.

Considering the close scores of the architectures in the trade-off analysis, as shown in Table 3, a more refined design of the plant components is necessary to make a well-informed choice. Nevertheless, a reduced batch of regolith that includes all the plant blocks appears to be the most effective solution. If a short or intermediate duration of the process is accepted, together with the complexity increase, it would be also possible to demonstrate the repeatability of the process.
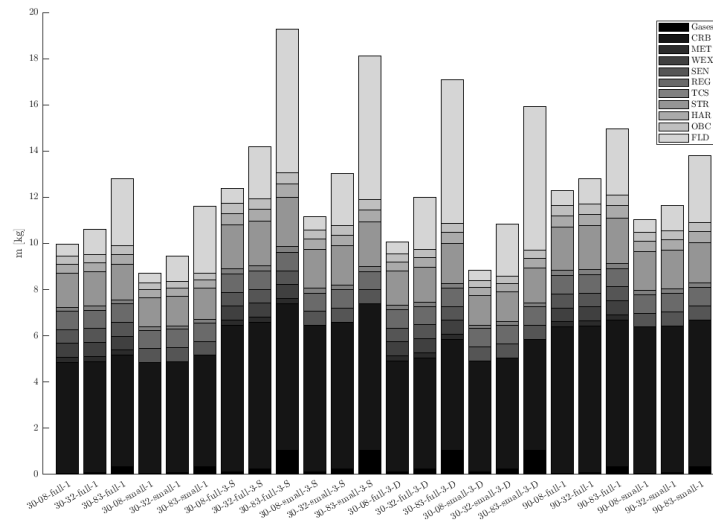
Figure 3: Mass budget of different possible architectures, with respect to the mass of the regolith batch (30-90g), the process duration (8-32-83h), the presence (*full*) or not (*small*) of the methanation and water extraction blocks, the number of process repetition (1-3) and the exhaust batch management strategy (*S* stacked or *D* discharge).

	Mass	Power	Sc. ret.	Complexity	TOT
30-08-full	3	3	1+1	3	11
30-32-full	3	3	1+1	3	11
30-83-full	2	2	2+1	3	10
30-08-full-3-S	2	2	2+1+1	2	10
30-32-full-3-S	2	2	2+1+1	2	10
30-83-full-3-S	1	1	3+1+1	2	9
30-08-full-3-D	3	3	2+1+1	1	11
30-32-full-3-D	3	3	2+1+1	1	11
30-83-full-3-D	2	2	3+1+1	1	10
90-08-full	2	2	2+1	3	10
90-32-full	2	2	2+1	3	10
90-83-full	1	1	3+1	3	9

Table 3: Architectures trade-off. Scores: mass 1 (heaviest)- 3 (lightest); power 1-3; scientific return 1 - 3 wrt yield, +1 for complete process demonstration, +1 for process repetitions; complexity 1-3 wrt number of mechanism.

4. The carbothermal reactor

The carbothermal reactor is the most critical component of the plant in terms of mass and power requirements. In this section, a preliminary configuration of the reactor is presented, along with thermal simulations performed to optimize it and minimize thermal losses.

The baseline configuration of the reactor involves a cylindrical chamber sized to accommodate the required mass of regolith at its centre. Sufficient space, at least two times the height of the regolith batch, is provided above the regolith to facilitate gas mixing. The inlet and outlet domains of the reaction chamber are designed with an inclination of 45-55° to facilitate the loading and unloading of the regolith. To reduce the power required for heating the regolith batch, one or more layers of insulation materials are being considered. The specific material, its thermal properties, and the number and thickness of these layers are the primary design parameters for the reactor: an overview of the material properties is given in Table 4. Additionally, an external chamber with a minimum thickness is added to enclose the reactor system in the full configuration. The thermal and structural behaviour of this chamber will depend on the final configuration of the plant. However, the detailed design and optimization of the external chamber are beyond the scope of this initial design iteration and will be addressed in subsequent steps.

| (a) Chamber only | (b) Insulation layers | (c) Full configuration |
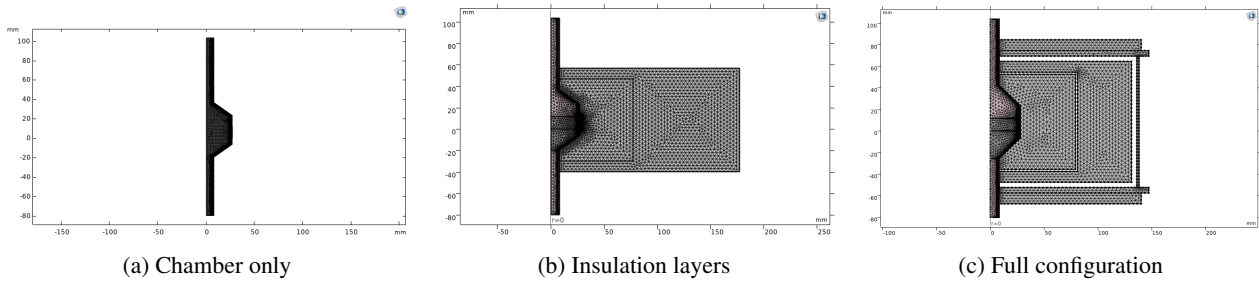
Figure 4: Carbothermal reactor configurations for thermal analysis and adopted mesh.

Materials	ρ [kg/m^3]	k [W/mK]	ϵ [-]
Regolith	1303	$1.281e-2+4.431e-10T^3$	0.01
Alumina	1950	$85.868-0.22972T+2.607e-4T^2-1.3607e-7T^3+2.7092e-11T^4$	0.8
Carbon aerogel	10	$0.1134+1.829e-4T$	0.5
Silica aerogel	150	0.02	0.4
Zirconium	6000	3	0.88
MLI	-	-	0.0245

Table 4: Parameters adopted for the thermal simulations of the component.

4.1 Preliminary thermal analysis

To optimize the geometric parameters of the selected reactor configuration and minimize thermal losses towards the environment, a thermal analysis using COMSOL Multiphysics was performed. The analysis was conducted in an incremental manner, starting from modelling the reaction chamber alone with thermal insulation on the external surfaces. Subsequently, the analysis included radiation towards the environment, insulation layers, and the external chamber. The configurations and adopted meshes for each step are shown in Figure 4. The parameters considered for the optimization were the reaction chamber diameter, the power supplied to the reactor, and the thickness of the two insulation layers. By iteratively adjusting these parameters, the aim was to enhance the thermal performance of the reactor and minimize heat loss during operation. The material properties adopted for the simulations are listed in Table 4.

CRB1 - Heating of the regolith batch. The first analysis focused on the heating of the regolith batch and the inner reaction chamber, as shown in Figure 4a. The model considered the regolith as a porous domain and the reaction chamber made of alumina. A gaseous domain was included in the inlet and outlet regions of the chamber, and adiabatic conditions were applied to all domain boundaries except for the gas domain ones, where the inlet temperature was imposed. The objective of the simulation is to verify the heating of the regolith within the given time frame of approximately 10 hours and assess the influence of the inner radius of the chamber and the power supplied. Figure 5a demonstrates that a power input of 12 W is sufficient to heat the batch from $-153\,°C$ to the desired reaction temperature. Additionally, the simulation indicated that the inner radius of the chamber does not significantly impact the heating time. However, when the adiabatic boundary condition was replaced with radiation towards the environment, as shown in Figure 5b (CRB-1-rad), the desired reaction temperature was not reached. This finding suggests, as expected, the need for external insulation layers and a higher power source to achieve the desired heating temperature.
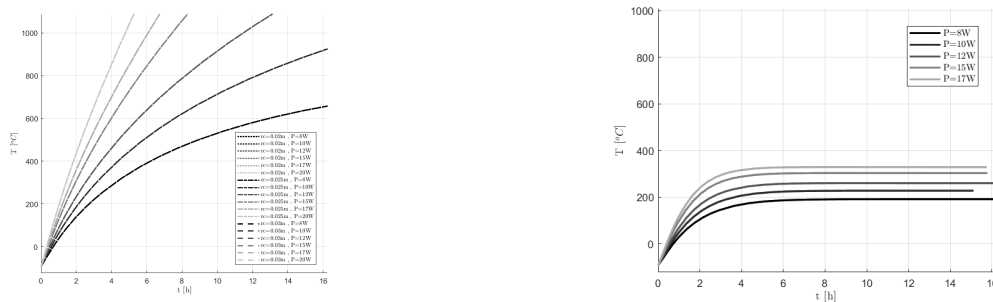
| (a) CRB-1, batch temperature vs chamber radius and power. | (b) CRB-1-rad, batch temperature vs chamber radius and power. |

Figure 5: Carbothermal reactor thermal analysis results - chamber only
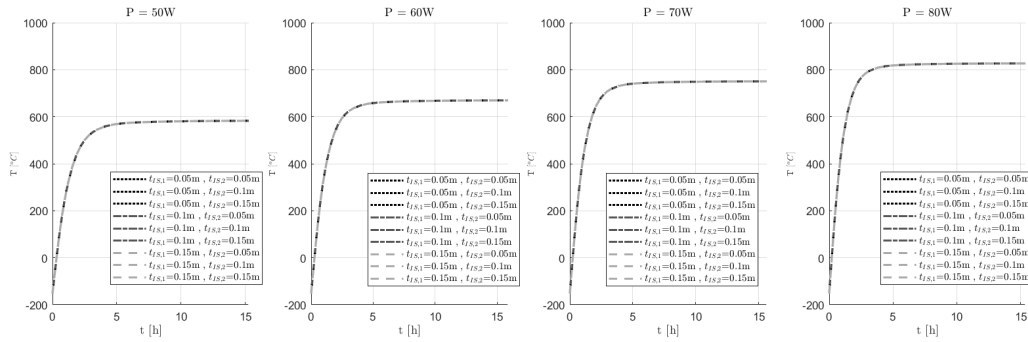
Figure 6: Carbothermal reactor thermal analysis results - insulation layers

CRB2 - Insulation layers. To reduce dissipation towards the external environment, two layers of insulant materials were added to the reactor chamber. The two types of insulants considered are carbon aerogels and silica aerogels. Carbon aerogels can withstand very high temperatures, up to 2000 °C, and their surfaces can be finished to reflect the radiation towards the hot part of the reactor. They can also serve a structural function. On the other hand, silica aerogels have insulation capabilities approximately one order of magnitude higher than carbon aerogels, but they cannot be used as structural components and can withstand temperatures of around 700 °C. Therefore, a carbon aerogel layer is considered closer to the chamber, while the outer layer is made of silica aerogel to further decrease the temperature. Figure 6 illustrates the simulation results for different thicknesses of the two insulation layers. The different thicknesses of the insulation layers impact the slope of the final heating phase and the plateau. However, similar to the previous case, the primary parameter that governs the temperature of the regolith batch is the power supply, which is still insufficient to reach the desired reduction temperature inside the chamber.

CRB3 - Radiation. Radiation cannot be neglected in the lunar environment; therefore, the complete model of the carbothermal reactor must include it: both the radiation with the external environment and within the reactor are taken into account. For the external surfaces, an emissivity value of $\epsilon = 0.02$ is assumed, representing the presence of a Multi-Layer Insulation (MLI) to minimize dissipation. Inside the reactor, vacuum regions are intentionally left between the insulation layers to minimize conduction between them; also here, the surfaces radiating towards the outside of the reactor are assumed to have an emissivity comparable to the one of the MLI. To fully represent the reactor, the external chamber is modelled around the second insulation layer. The complete configuration is depicted in Figure 4c with the mesh adopted for the computations. As mentioned, heat transfer through solids, fluids, porous media, and radiation is modelled using a transient study to achieve and maintain the reduction temperature starting from ambient conditions.

The main parameters investigated in this study are the power of the heater and the geometry of the insulation layers. The impact of the thickness of the different layers is relatively small compared to the effect of power increase, which has a predominant influence on the batch temperature as can be seen in Figure 7b. The temperature distribution in the carbothermal reaction after the end of the heating phase is shown in Figure 7a, where the reaction temperature is reached inside the regolith batch starting from an initial temperature of -153 °C and utilizing a power source of 100 W. Additionally, this setup takes advantage of the beneficial effect of increased vacuum spaces between the insulation layers. The results highlight the critical importance of the power input to achieve the desired temperature within the regolith batch. Moreover, the configuration with increased vacuum spaces between insulation layers demonstrates improved thermal performance. These findings emphasize the need to optimize the power supply and insulation design to ensure efficient carbothermal reduction in the lunar environment.

CRB4 - Process phase. Once the configuration is established, the behaviour of the reactor is studied during the process phase. The initial conditions are changed: the batch temperature, the heater and the reactor chamber are supposed to be at the process temperature, at about 1100 °C, while the remaining layers of the plant are assumed to be at 200 °C. Figure 8a shows the results of a stationary analysis given the aforementioned boundary conditions. A power source of 45 W is imposed. The reaction temperature is reached almost uniformly in the regolith batch, while it remains high at the gas outlet, meaning that the design of this region of the furnace shall be improved to be compliant with the sealing requirement. Figure 8b illustrate instead the results of a transient analysis, with the same settings of the stationary. The evolution of the average batch temperature and the power source are shown. For the latter a binary control is added: the heat source is on until the batch temperature reaches the limit value of 1200 °C, then it is switched off until the batch is cooled to the process temperature. Also in this case it can be seen that the regolith batch is properly kept at the process temperature for the whole duration of the process.

(a) Temperature distribution after 15 hours process (P=100 W, r_c=2 cm).

(b) Temperature profiles with respect to different power values.
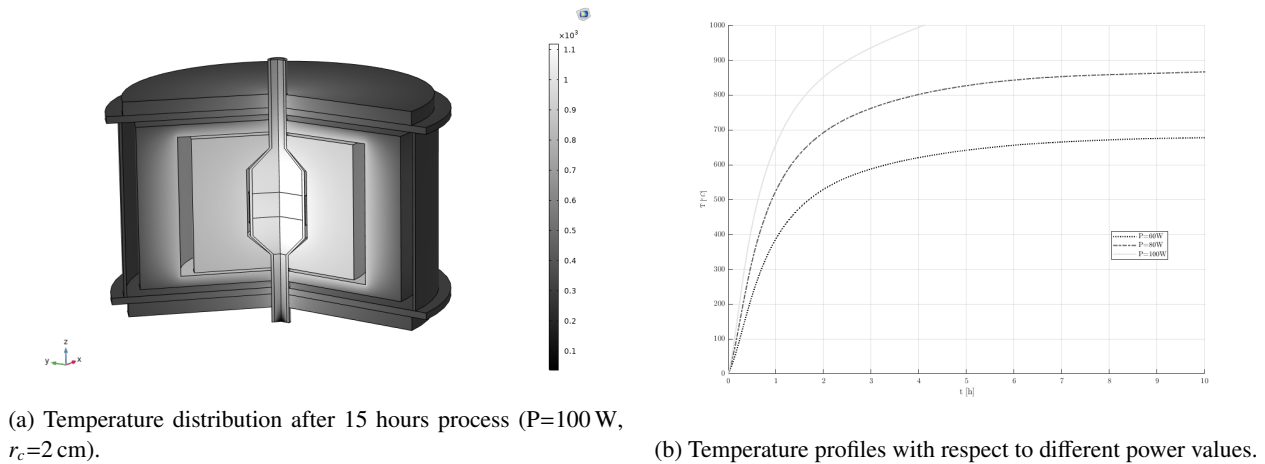
Figure 7: Carbothermal reactor thermal analysis results - full configuration

(a) Temperature distribution in the process phase (stationary analysis, T_0=1000°C).

(b) Temperature evolution during a 32h process with P=45W and an initial temperature of 1000°C
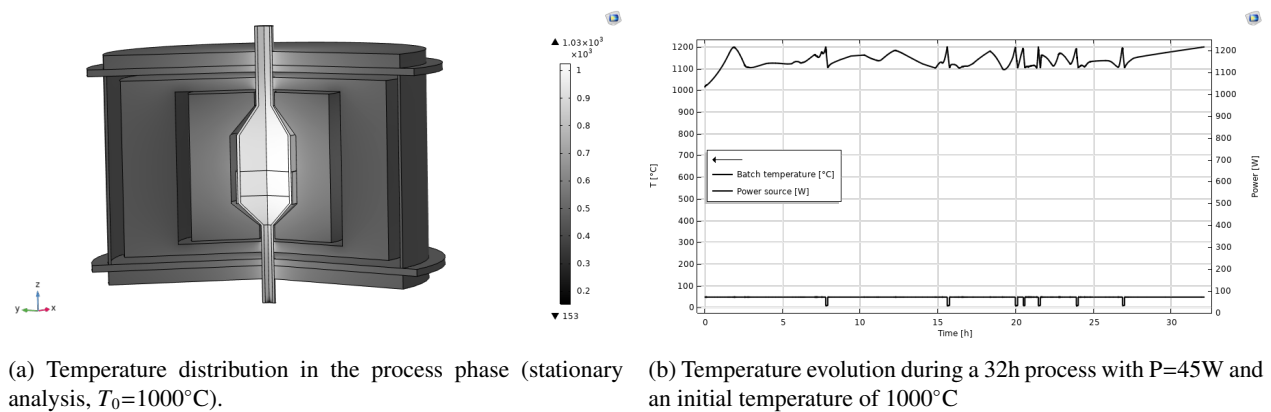
Figure 8: Carbothermal reactor thermal analysis results - full configuration, process phase

Complete thermal analysis   Finally, a full simulation is performed, considering both the heating and the oxygen extraction phase. The configuration is the same as the one adopted in the process phase analysis, as well as the materials. A power source of 65W is exploited both in the heating and in the process phase to successfully reach and maintain the carbothermal reduction temperature inside the regolith batch. Figure 9b illustrates the evolution with respect to time of the average temperature of the regolith batch: it can be seen that after about 10h the temperature is the reaction one, as shown also in Figure 9a; the reduction temperature is maintained for the whole duration of the process: in this phase, the binary control presented in the process phase results is active. This outcome successfully achieves the required operating temperature while meeting the power availability limitations imposed by some of the CLPS landers; however, it excludes others such as the Astrobiotics lander. The analyses conducted demonstrate that the chosen configuration and geometry fulfil the requirements while highlighting the significance of the thermal and optical insulant material properties: these properties play a crucial role in significantly reducing the power demand.

Mass evaluation.   The mass of the reactor is directly evaluated in COMSOL Multiphysics on the presented configurations. Given the densities listed in Table 4 and the configuration of Figure 7b, the masses of the different layers result to be: $m_{CA} = 0.0196$kg, $m_{SA} = 0.34796$kg, $m_{reg} = 0.0626$kg, $m_{chamb} = 0.04329$kg, $m_{zi} = 2.936$kg. The total mass of the reactor, with a 50% margin applied, results to be 5.20 kg, aligned with the value adopted in the architecture trade-off. This mass does not include any loading or unloading valves and mechanisms.

Criticalities   The high power required to heat and maintain the reactor at the operating temperature restricts the choice of suitable landers for the mission. To mitigate dissipation and reduce power demand, alternative solutions can be explored, such as incorporating reflecting surfaces to confine heat towards the reactor or investigating different materials for the insulation layers and configurations. Additionally, the flanges used for sealing the reactor typically have a temperature limit of around 400 °C. If the temperature of the gas at the reactor outlet exceeds this limit,
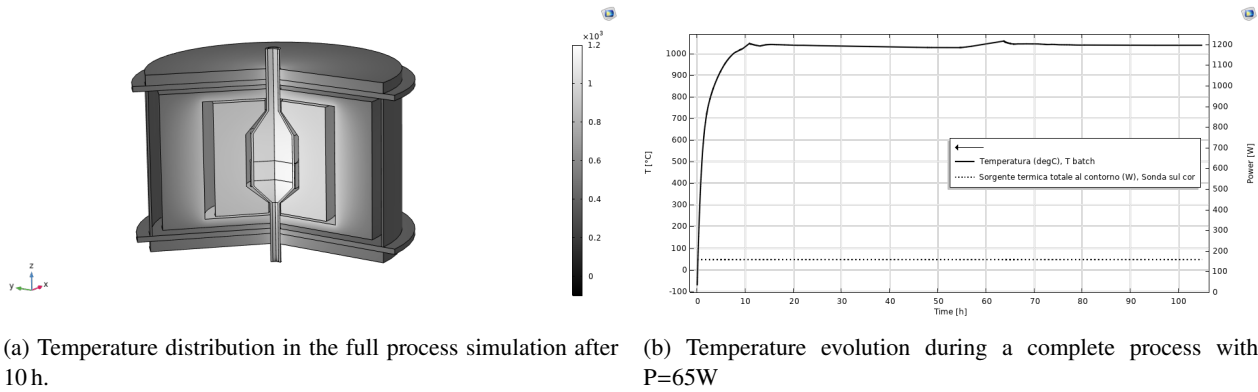
(a) Temperature distribution in the full process simulation after 10 h.

(b) Temperature evolution during a complete process with P=65W

Figure 9: Carbothermal reactor thermal analysis results - full configuration, process phase

alternative solutions need to be considered. While metallic flanges can withstand higher temperatures, they are not reusable, which eliminates the possibility of a repeated process.

5. Other components

5.1 Methanation reactor.

The methanation reactor needs to be appropriately sized to ensure complete conversion of CO. The 2018-2021 experimental campaign on the laboratory plant, along with existing literature,[22] have been used to model the chemistry and species transport within the reactor under different flow conditions. Based on this information, the minimum reaction length required for complete CO conversion, with an adequate margin, can be computed. In Figure 10 are shown the dependences of the length with respect to the pressure and temperature conditions and with respect to the inlet mass fraction of carbon monoxide e methane. Figure 10 illustrates the dependence of the reactor length on pressure, temperature, and inlet mass fraction of carbon monoxide and methane. Higher reaction temperatures favor the methanation reaction and require a shorter reactor length. However, temperatures above 250 °C can lead to catalyst degradation and methane dissociation. Similarly, a higher concentration of CO necessitates a longer reactor length for complete conversion. As a baseline, a reactor length of 8 cm is considered, ensuring that at 1 atm and 250 °C, CO concentrations below 10% are fully converted.
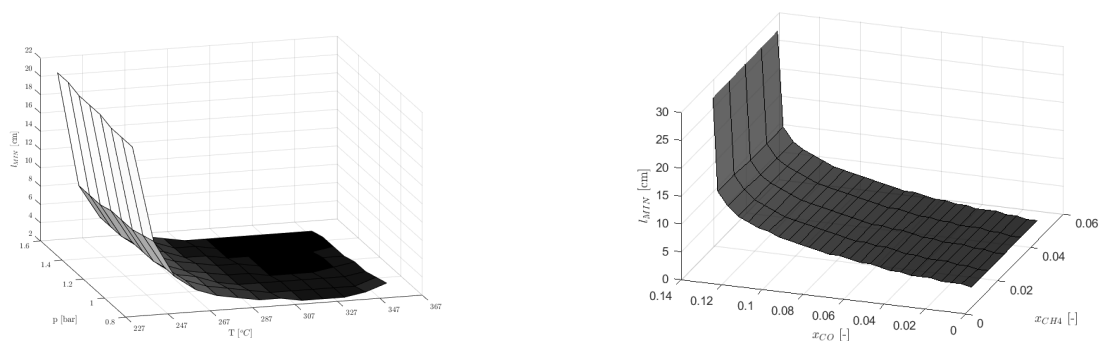
(a) Minimum methanation length with respect to pressure and temperature

(b) Minimum methanation length with respect to inlet molar fraction of CO and CH₄.

Figure 10: Minimum length required for the methanation reactor to fully convert CO under different process conditions.

Preliminary thermal analysis   Although the methanation reactor is smaller and has lower temperature requirements compared to the carbothermal reactor, it remains one of the most critical components in terms of power request. Therefore, it is important to closely examine its thermal behaviour.

A model of the methanation reactor was developed using COMSOL Multiphysics. As mentioned, to host the methanation reactions is chosen as a baseline a reactor similar to the carbothermal one. The model considers a cylindrical reaction domain filled with porous catalyst pellets and a flowing gas mixture. An external chamber with a heater and an insulation layer made of silica aerogel are included to reduce heat dissipation. Radiative heat exchange with the external environment occurs at the external surface, and the inlet gas flow is set to 70 °C. A power source of 8 W is applied at the interface between the reaction domain and the reactor chamber to simulate the heating coils. Figure 11a presents the results of a 10 h simulation: the reaction domain reaches the target temperature of 250 °C, which is nearly uniformly distributed in the second part of the domain. However, the effect of the low-temperature inflow gases is felt at the inlet. To address this, the catalyst pellets are placed a few centimetres after the reactor inlet, ensuring that they are maintained at the reaction temperature. The thickness of the insulation layer is arbitrarily set to 2 cm, but its value can be tuned accordingly to the final plant configuration to optimize the methanation reactor mass and thermal dissipation.
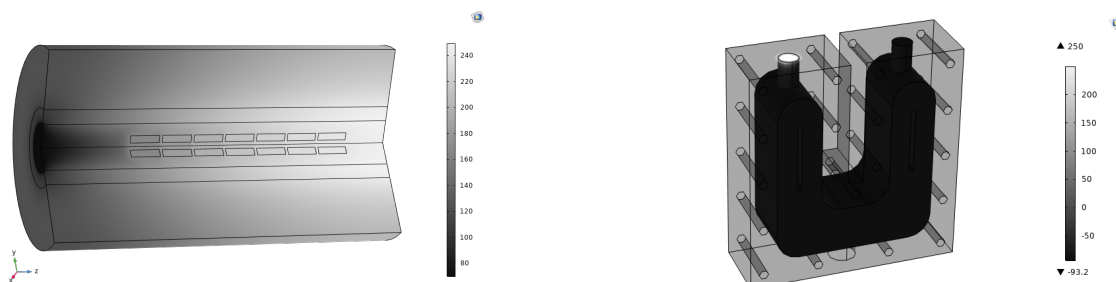
(a) Temperature distribution in the methanation reactor after 10 h of process.

(b) Temperature distribution of the condenser based on the terrestrial concept[26] facing the external lunar environment

Mass evaluation. The mass of the methanation reactor is directly evaluated in COMSOL Multiphysics, as for the carbothermal reactor. Given the configuration shown in Figure 11a, it results in a mass of 0.309 kg for the reactor chamber, made of AISI 316L, and a mass for the silica aerogel insulant layer of 0.052 kg; the mass of the catalyst pellets if few grams, so the total mass is 0.5 kg, with a 50% margin applied. This value is similar to the one adopted in the initial architecture mass budget computation.

5.2 Water extraction unit

The baseline design for the water extraction unit incorporates a condenser that exploits the lunar environment to solidify water vapour and store it in a dedicated container.

The geometry of the condenser will depend on the plant configuration and on the expected mass of water produced; in any case, a U-shape geometry can be considered, as the heritage of the knowledge gained with the terrestrial demonstrator,[26] with some changes to improve the performances of the terrestrial condenser, avoiding, for example, the formation of ice at the inlet. Figure 11b shows that the water vapour condensation conditions are met assuming that the condenser exchanges it with an environment at −93 °C. This ensures the preliminary feasibility of the water extraction unit, whose final configuration will depend on the other plant components, the lander architecture and operation timelines: it is unlikely that the lunar night temperature could be exploited because almost all the CLPS landers restrict the operations to the lunar day. So, to avoid the requirement for a refrigeration system, the condenser shall be wisely placed as far as possible from the demo plant's hot elements, i.e. the reactors, and possibly facing a shadowed region of the external surface.

5.3 Fluidics

The fluidic system plays a crucial role in connecting the different components of the plant and facilitating the flow of gases from the tanks to the reactors. The main elements to consider, depicted in Figure 12, include: pipes and adapters between the different elements; p ressure reducer to transition from the high-pressure tanks (operating at 200-300 bar) to the reactors, which operate at approximately 1 bar; mass flow controller, to select the correct flowrate of the species; check valves, to prevent unexpected back-flow of gases; flame arrestor, to ensure safety and prevent potential damages.

LUNAR ISRU PILOT PLANT DESIGN
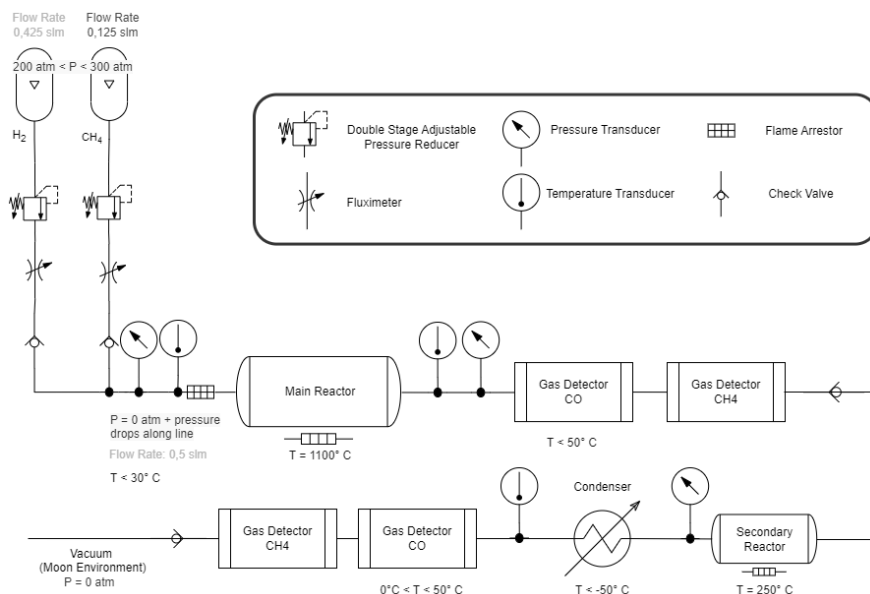
Figure 12: Full plant fluidic scheme. The number of process stages and sensors is subject to a trade-off, as explained in the text.

Criticalities   In principle, the fluidic system does not present significant challenges, as the required components are readily available off-the-shelf and have already been utilized in the PoliMi demonstrator plant.[26] However, the main challenge lies in the miniaturization of these components to meet the requirements of the compact plant design. The pressure reducer is the heaviest among the components, weighing around 1-1.5 kg. The higher the inlet pressure, the higher the reduced pressure, that then has to be compatible with the mass flow controller requirements. For instance, this device that is used for satellites propulsion regulation[9] is able to go from a maximum of 276 bar to 16 bar, that however is not compatible with one of the most compact flow controller,[5] that requires a maximum pressure of 10 bar (mass: 100-160 g; flowrate 0.2 ml/min to 5 l/min). Therefore, it may be necessary to select pressure reduction devices, similar to those used in the PoliMi tanks, capable of transitioning from 200 bar to 0-10 bar. The idea is, in any case, to start an interaction with the producers to select a device with a fixed reduction ratio: this should allow the removal of not necessary elements that would allow a manual regulation. It was also considered to integrate the pressure reduction stage with the flow control, but no valves capable of sustaining the required pressure drop were found. Flame arrestors weigh below 200 g (e.g.[34]), comparable to the mass of the flow controllers, while check valves pose no significant issue, weighing less than 20 g. Excluding pipes and adapters, the estimated mass of these elements for each line is approximately 1.44 kg (pressure reducer 1 kg; flow controller 0.16 kg; flame arrestor 0.191 kg, even if one is enough for both; check valve 0.02 kg; 5 % margin on top). When considering the estimated tank mass, which can reach up to 2 kg for the 83-hour process, the contribution of the fluidic subsystem to the overall mass budget of the demo plant becomes significant. Therefore, it is necessary to collaborate with manufacturers to explore potential solutions for reducing the mass of these devices and allocate more of the mass budget to the plant payloads.

5.4 Measurement and monitoring

The measurement components are essential in collecting scientific data to assess the process yield, while the monitoring components ensure the proper functioning of the system by monitoring pressure and temperature.

One viable option for measuring the CO and CH_4 molar fraction is the use of infrared gas sensors, leveraging the heritage of the MOXIE experiment.[13] Each sensor has a mass of 0.087 kg and dimensions of 76 mm x 30 mm x 50 mm, with a power requirement of $\leq$ 800 mW, and are capable of monitoring real-time flow rates similar to those employed in the plant.[30] While suitable for use with hydrogen, one limitation is their reliance on atmospheric conditions for the measurement. Alternatively, electrochemical detection sensors can be adopted as an alternative choice.[1] These sensors offer similar performances and drawbacks, such as the atmospheric conditions for the measurements. Pressure and temperature along the fluidic lines are monitored to ensure proper flow within the plant. Pressure information is crucial for control logic to prevent overpressures in the reactors. Transducers are placed before and after each stage, as shown in Figure 12. Temperature information in the pipes helps identify potential issues and cross-checks the expected values from the models. The mass of COTS pressure and temperature sensors remains below 100 g for each element.

To measure the mass of the regolith batch loaded in the reactor several sensors with different technologies can be exploited, as mentioned before. Level sensors, commonly used in terrestrial applications to measure the height of granular materials, and so exploitable to measure the volume of the regolith batch, come in different technologies such as piezoelectric,[32] microwave,[33] radar, and ultrasonic. Of these, piezoelectric and microwave sensors are the most suitable for measuring in the order of centimeters. They have minimal power requirements and operate within a wide range of temperatures. However, it's important to note that the insertion of a piezoelectric sensor probe inside the reactor may compromise its sealing capability. Otherwise, load cells can be used to measure both the mass of the regolith batch and the mass of the produced water, if the methanation and water extraction blocks are present.

Criticalities The presented gas sensor has a TRL (Technology Readiness Level) of 9, having already flown in the MOXIE experiment and being used in the International Space Station. There are no significant issues with these sensors as they are small, low power-consuming, and lightweight. However, it should be noted that they operate in ambient conditions with a certain level of humidity, which needs to be replicated in the lunar environment.

As for the other components, also for the pressure and temperature monitoring the idea is to reduce at the most their mass. As previously highlighted, the pressure transducers are essential to prevent overpressures, and so damage to the components. On the other hand, a trade-off can be made for temperature monitoring between their necessity and the mass they contribute. Instead of in-line transducers, conventional miniature thermocouples can be placed at strategic points directly on the pipes. This approach allows for temperature differences to be evaluated in relation to background values measured before the process starts.

6. Conclusion

Various process strategies and plant architectures have been proposed to demonstrate the carbothermal reduction in the lunar environment while meeting the constraints of commercial landers planned for lunar missions. Preliminary considerations were made regarding mass and power budgets, scientific value, and the complexity of each strategy and architecture. Based on these factors, it is suggested that a demonstration of the process with a small regolith batch and all the plant components may be a more favourable solution than focusing solely on carbothermal reduction using a large regolith batch. However, further analysis and trade-offs are required to refine the selection of plant components due to their complexity.

A thermal model of the carbothermal reactor was presented to guide the selection of an optimal geometry that minimizes power requirements. The power demand for heating the regolith to the reduction temperature emerged as a significant challenge in the plant design, and potential solutions were proposed to address this issue. A careful selection of the insulant materials and solution to maximise the containment of the heat inside the reaction chamber will allow the fulfilment of the plant requirements while staying in the lander capabilities. The second major challenge in realizing the lunar demonstration plant is the miniaturization of fluidic components, particularly pressure reducers. However, this criticality can be tackled including component design improvements and adaptations of existing terrestrial solutions. Overall, all the functionalities for the carbothermal process demonstration can be accomplished; a scheme of the full plant is proposed in Figure 12 together with the design of the payloads.

References

[1] Angst+Pfister. URL: TB200B-ES1/ES4-CO-10%-01 Technical Specifications . (Last access: june 2023).

[2] Astrobotic data. URL 1: https://www.astrobotic.com/lunar-delivery/landers/peregrine-lander/, URL 2 https://www.astrobotic.com/wp-content/uploads/2022/01/PUGLanders_011222.pdf. (Last access: feb 2023).

[3] V. Badescu, K. Zacny, and Y. Bar-Cohen, editors. *Handbook of Space Resources*. Springer International Publishing, 1 edition, 4 2023.

[4] Blue Origin data. URL 1: https://www.blueorigin.com/blue-moon/, URL 2 https://www.space.com/blue-origin-blue-moon-lander-explained.html. (Last access: feb 2023).

[5] Bronkhorst. URL: https://www.bronkhorst.com/int/products/gas-flow/iq-flow/iqf-100c/?pdf=true . (Last access: june 2023).

[6] Kevin M. Cannon, Christopher B. Dreyer, George F. Sowers, John Schmit, Thao Nguyen, Keoni Sanny, and Joshua Schertz. Working with lunar surface materials: Review and analysis of dust mitigation and regolith conveyance technologies. *Acta Astronaut.*, 196:259–274, 7 2022.

[7] Ceres Robotics data. URL: https://www.ceresrobotics.com/products-1. (Last access: feb 2023).

[8] Draper data. URL 1: https://www.draper.com/news-releases/draper-returns-moon-enables-future-exploration, URL 2 https://www.draper.com/sites/default/files/2019-08/Artemis-7_PUG_0.pdf. (Last access: feb 2023).

[9] Eaton. URL: https://www.eaton.com/us/en-us/catalog/aerospace-valves/satellite-propulsion-regulator.specifications.html . (Last access: june 2023).

[10] Firefly data. URL 1: https://firefly.com/blue-ghost/, URL 2 https://firefly.com/wp-content/uploads/2022/01/Blue_Ghost_PUG-1.pdf. (Last access: feb 2023).

[11] R. Gustafson, B. White, M. Fidler, and A. Muscatello. Demonstrating the Solar Carbothermal Reduction of Lunar Regolith to Produce Oxygen. *48th AIAA Aerospace Sciences Meeting Including the New Horizons Forum and Aerospace Exposition, 4 - 7 January 2010, Orlando, Florida, AIAA 2010-1163*, pages 4–12, 2010.

[12] J. Han, J. Feng, P. Chen, Y. Liu, and X. Peng. A review of key components of hydrogen recirculation subsystem for fuel cell vehicles. *Energy Convers. Manag.: X*, 15, 8 2022.

[13] M. Hecht, J. Hoffman, D. Rapp, J. McClean, J. SooHoo, R. Schaefer, A. Aboobaker, J. Mellstrom, J. Hartvigsen, F. Meyen, E. Hinterman, G. Voecks, A. Liu, M. Nasr, J. Lewis, J. Johnson, C. Guernsey, J. Swoboda, C. Eckert, C. Alcalde, M. Poirier, P. Khopkar, S. Elangovan, M. Madsen, P. Smith, C. Graves, G. Sanders, K. Araghi, M. de la Torre Juarez, D. Larsen, J. Agui, A. Burns, K. Lackner, R. Nielsen, T. Pike, B. Tata, K. Wilson, T. Brown, T. Disarro, R. Morris, R. Schaefer, R. Steinkraus, R. Surampudi, T. Werne, and A. Ponce. Mars Oxygen ISRU Experiment (MOXIE). *Space Sci. Rev.*, 217:1–76, 2 2021.

[14] G. Heiken, D.T. Vaniman, and B.M. French. *Lunar Sourcebook: A user's guide to the Moon*. Cambridge University Press, 1991.

[15] J. A. Hoffman, M. H. Hecht, D. Rapp, J. J. Hartvigsen, J. G. SooHoo, A. M. Aboobaker, J. B. McClean, A. M. Liu, E. D. Hinterman, M. Nasr, S. Hariharan, K. J. Horn, F. E. Meyen, H. Okkels, P. Steen, S. Elangovan, C. R. Graves, P. Khopkar, M. B. Madsen, G. E. Voecks, P. H. Smith, T. L. Skafte, K. R. Araghi, and D. J. Eisenman. Mars Oxygen ISRU Experiment (MOXIE) - Preparing for human Mars exploration. *Sci. Adv.*, 8(35):eabp8636, 2022.

[16] Intuitive Machines data. URL 1: https://space.skyrocket.de/doc_sdat/nova-c.htm, URL 2 https://bsgn.esa.int/wp-content/uploads/2022/08/Lunar-Economy-Workshop_Lunar-Payload-Delivery-Services.pdf, URL 3: https://www.intuitivemachines.com/lunar-access-services, URL 4 https://www.intuitivemachines.com/_files/ugd/7c27f7_458cf85ba6e94ba18f33702dc2c326af.pdf. (Last access: feb 2023).

[17] C. Junaedi, K. Hawley, D.Walsh, S. Roychoudhury, M. B. Abney, and J. L. Perry. Compact and Lightweight Sabatier Reactor for Carbon Dioxide Reduction. 2011.

[18] D. Knez and M. Khalilidermani. A Review of Different Aspects of Off-Earth Drilling. *Energies*, 14:7351, 11 2021.

[19] Lockheed Martin Space data. URL 1: https://www.lockheedmartin.com/en-us/products/mccandless-lunar-lander.html, URL 2 https://cdn2.hubspot.net/hubfs/517792/Space/McCandless_Lander_User_Guide_Release1.pdf. (Last access: feb 2023).

[20] Masten data. URL 1: https://explorers.larc.nasa.gov/2019APSMEX/MO/pdf_files/Masten%20Lunar%20Delivery%20Service%20Payload%20Users%20Guide%20Rev%201.0%202019.2.4.pdf. (Last access: feb 2023).

[21] A. Meurisse, B. Lomax, A. Selmeci, M. Conti, R. Lindner, A. Makaya, M. D. Symes, and J. Carpenter. Lower temperature electrochemical reduction of lunar regolith simulants in molten salts. *Planet. Space Sci*, 211:105408, 2022.

[22] C.V. Miguel, A. Mendes, and L.M. Madeira. Intrinsic kinetics of CO2 methanation over an industrial nickel-based catalyst. *J. CO2 Util.*, 25:128–136, 2018.

[23] Moon Express data. URL 1: https://moonexpress.com/, URL 2 https://www.hou.usra.edu/meetings/leag2017/presentations/wednesday/spudis.pdf. (Last access: feb 2023).

[24] NASA Solicitation and Proposal Integrated Review and Evaluation System. URL: https://nspires.nasaprs.com/external/index.do;jsessionid=QOde-TTDWWJ-uswCvRWtdwhk7NnGJuRD0wbP361MKV9ij0gB3pUn!199331103!wnp2.nasaprs.com!7006!-1!1962942317!wnp1.nasaprs.com!7006!-1. (Last access: feb 2023).

[25] Planned mission reference data. URL 1: https://www.planetary.org/space-missions/clps#: :text=Upcoming%20CLPS%20Moon%20landings,Astrobotic%20(now%20delayed%20to%202023); URL 2: https://www.eoportal.org/other-space-activities/clps#the-nine-instruments-to-be-delivered-are; URL 3: https://www.nasa.gov/press-release/nasa-selects-firefly-aerospace-for-artemis-commercial-moon-delivery-in-2023 (Last access: feb 2023).

[26] J. Prinetto, A. Colagrossi, A. Dottori, I. Troisi, and M. R. Lavagna. Terrestrial demonstrator for a low-temperature carbothermal reduction process on lunar regolith simulant: Design and AIV activities. *Planet. Space Sci.*, 2022.

[27] D. J. Samplatsky, K. Grohs, M. Edeen, J. Crusan, and R. Burkey. Development and integration of the flight Sabatier assembly on the ISS. American Institute of Aeronautics and Astronautics Inc., 2011.

[28] H. M. Sargeant, F. A.J. Abernethy, M. Anand, S. J. Barber, P. Landsberg, S. Sheridan, I. Wright, and A. Morse. Feasibility studies for hydrogen reduction of ilmenite in a static system for use as an ISRU demonstration on the lunar surface. *Planet. Space Sci.*, 180:104759, 1 2020.

[29] L. Schlüter and A. Cowley. Review of techniques for In-Situ oxygen extraction on the moon. *Planet. Space Sci.*, 181:104753, 2020.

[30] SmartGas. URL: SmartGas FlowEVO Infrared Gas Sensor . (Last access: june 2023).

[31] I. Troisi, P. Lunghi, and M. R. Lavagna. Oxygen extraction from lunar dry regolith: Thermodynamic numerical characterization of the carbothermal reduction. *Acta Astronaut.*, 199:113–124, 2022.

[32] UWT GmbH. URL: Piezoresistive level sensor . (Last access: june 2023).

[33] UWT GmbH. URL: Microwave level sensor. (Last access: june 2023).

[34] WittGas. URL: https://www.wittgas.com/products/gas-safety-equipment/flashback-arrestors-flame-arrestors/for-pressure-regulators-outlet-points-inline/flashback-arrestor-rf53n/ . (Last access: june 2023).

[35] X. Zhang, G. Zhang, H. Xie, M. Gao, and Y. Wen. A Review of Sampling Exploration and Devices for Extraterrestrial Celestial Bodies. *Space Sci. Rev.*, 218:1–50, 10 2022.